S. L. Dudarev, P. Liu, D. A. Andersson, C. R. Stanek,
T. Ozaki, C. Franchini

Parameterisation of an LSDA+U model for non-collinear magnetic configurations

Parameterisation of an LSDA+U model for non-collinear magnetic configurations

S. L. Dudarev, P. Liu, D. A. Andersson, C. R. Stanek, T. Ozaki, C. Franchini

Parameterisation of an LSDA+U model for non-collinear magnetic configurations: Multipolar magnetism in UO$_2$

S. L. Dudarev,[1, *] P. Liu,[2] D. A. Andersson,[3] C. R. Stanek,[3] T. Ozaki,[4] and C. Franchini[2, 5, †]

[1] *UK Atomic Energy Authority, Culham Centre for Fusion Energy, Oxfordshire OX14 3DB, United Kingdom*
[2] *University of Vienna, Faculty of Physics and Center for Computational Materials Science, Sensengasse 8, A-1090 Vienna, Austria*
[3] *Materials Science and Technology Division, Los Alamos National Laboratory, Los Alamos, New Mexico 87545, USA*
[4] *Institute for Solid State Physics, The University of Tokyo, Kashiwa 277-8581, Japan*
[5] *Dipartimento di Fisica e Astronomia, Università di Bologna, 40127 Bologna, Italy*

Unraveling the complexity of non-collinear magnetism in materials with strongly correlated electrons is a considerable task that requires developing and applying state of the art theories and computational methods. Using the Coury model Hamiltonian, which includes spin and orbital degrees of freedom and generalizes the collinear Stoner Hamiltonian, we derive an extension of the collinear LSDA+U approximation to non-collinear magnetic configurations and explore the magnetic ground state of the archetypal spin-orbit correlated oxide UO$_2$. We show that parameterizing a non-collinear LSDA+U model requires only one parameter U, as opposed to the difference between the Hubbard and Stoner parameters $U - J$ found in an earlier derivation based on a collinear model Hamiltonian. To find the magnetic ground state of UO$_2$ in the non-collinear configuration space, we combine LSDA+U with a spin adiabatic occupation matrix approach, involving the construction of a magnetic energy surface that follows the adiabatic evolution of the occupation matrix as a function of the spin canting angle. Our results show that the strong spin-orbit coupling (SOC) is the key factor stabilizing the so-called 3**k** spin ordered magnetic ground state of UO$_2$. Using a relativistic atomic Hamiltonian we find that the SOC strength is colossal, 1.49 eV per uranium atom, the largest value ever found in relativistic materials. This unusually strong SOC implies that the spin and orbital degrees of freedom are virtually inseparable. As a result, to derive and quantify spin-spin interactions it is necessary to adopt the pseudospin picture. By constructing an extended effective multipolar pseudospin Hamiltonian, we prove the significance of octupolar and dipole-dipole exchange couplings in establishing the 3**k** magnetic phase, consistent with the non-collinear spin arrangement, and associated with the non-canted orbital ordering of uranium f-orbitals. Importantly, our study reveals that despite the strong spin-lattice interactions in action in UO$_2$, the cooperative Jahn-Teller instability does not contribute to the onset of the non-collinear 3**k** state, which remains the most favorable ground state even in the undistorted cubic lattice. Finally, we discuss the role of prefactor U in the LSDA+U scheme and provide evidence that the choice of this parameter has a substantial quantitative influence on the predicted properties of the oxide, in particular the magnetic exchange interactions and, perhaps trivially, on the band gap: the value of U computed fully *ab initio* by the constrained random phase approximation, U=3.46 eV, delivers a band gap of 2.11 eV in good agreement with experiment, and a balanced account of the other relevant energy scales.

I. INTRODUCTION

A realistic treatment of magnetic properties by *ab initio* methods requires using approaches that do not artificially constrain the orientation of magnetic moments to a specific direction. This is achieved by means of the so-called non-collinear density functional theory approximation [1, 2]. In the non-collinear approximation, the direction of the local magnetic moment varies from point to point in real space, and the fact that magnetic non-collinearity does indeed occur in real materials is confirmed by direct experimental observations [3–6]. Non-collinear spin orderings is particularly evident in heavy element compounds where it results from strong spin-orbit coupling effects. Examples include f-electron systems [7–9] and 5d transition metal oxides [10, 11]. Fluctuations of magnetic non-collinearity is a factor contributing to electrical and thermal resistivity of alloys [12] and may offer a clue to understanding electronic and magnetic phase transitions [13, 14]. It has also been discovered that non-collinear magnetic fluctuations may be responsible for the observed anomalous thermal conductivity of uranium dioxide [15], a material of considerable technological significance. Indeed, while in metallic alloys, magnetic fluctuations represent just one of the types of electronic excitations associated with the electric and thermal resistivity of the material, in a semiconducting oxide like UO$_2$, where thermal conductivity is dominated by the transport of phonons, the strong spin-orbit coupling (SOC) linking atomic displacements with magnetic degrees of freedom provides an additional and potentially significant channel of dissipation. The fact that lattice and magnetic degrees of freedom in uranium dioxide are strongly coupled has been confirmed by

* sergei.dudarev@ukaea.uk
† cesare.franchini@univie.ac.at

observations of piezo-magnetism [16]. The observations were modeled phenomenologically, assuming the occurrence of direct coupling between atomic displacements and magnetic moments. On the electronic structure level, such a coupling stems from the relativistic SOC between the magnetic moments of uranium ions and their orbital degrees of freedom, where the relatively weak but still notable directional character of bonds involving valence f-orbitals of uranium ions generates inter-atomic forces that depend on the orientation of magnetic moments.

The fundamental difference between a magnetic metal and an actinide oxide like UO_2 is that while the spin-orientation-dependent forces in a metal stem from the coordinate dependence of the Heisenberg exchange [17], in an antiferromagnetic semiconducting actinide oxide the forces result from a combination of Anderson's superexchange [18, 19], the strong correlations between electrons occupying f-shells of uranium atoms [20], and the relativistic spin-orbit interaction [21–23] coupling magnetic configurations to forces acting on the nuclei. In what follows, we shall focus on exploring the electronic and magnetic aspects of the problem using a suitably adapted *ab initio* LSDA+U model.

The subtlety of the problem is associated with the fact that the *ab initio* approach to the treatment of directional magnetic degrees of freedom in materials with strongly correlated electrons requires a non-collinear formulation of the electronic structure model, which at the same time must be suitable for the evaluation of the total energy of the electronic system. A LSDA+U model often applied to total energy calculations [24] has been derived from a collinear model Hamiltonian, similar to the Hamiltonians used earlier by Anisimov *et al.* [25] and by Kotani and Yamazaki [20]. It can be readily shown that these model Hamiltonians are identical to the Hamiltonian of the collinear Stoner model [26], and hence do not provide a suitable foundation for the treatment of noncollinear magnetism. A LSDA+U model that can in principle be applied to the treatment of non-collinear magnetism was proposed by Liechtenstein *et al.* [27]. However the choice of the double counting term, which has the same form as in the collinear case, *cf.* equation (4) of Ref. [27] and equation (3) of Ref. [26], introduces an element of uncertainty in the total energy part of the analysis.

The choice of the LSDA+U model for the analysis below is stimulated by the extensive application of *ab initio* approaches to the simulation of materials with strongly correlated electrons [28–33]. In what follows, we explore a generalization of the collinear LSDA+U model [24] to non-collinear magnetic configuration.

The new development has been stimulated and enabled by a recent work by Coury *et al.* [34] who found a way of transforming, through an exact calculation, the general four-index matrix form of the second-quantized Hamiltonian for interacting electrons, into a simpler form, resembling the Hamiltonian used earlier for the derivation of simplified versions of the LSDA+U model [24, 25]. The relative simplicity of the Coury Hamiltonian enables

performing a more accurate derivation of the LSDA+U model suitable for the treatment of non-collinear magnetism in materials with strongly correlated electrons, at the same time providing means for deriving a double counting term for the total energy calculations.

Below we apply the method to the investigation of electronic structure and non-collinear magnetism in uranium dioxide. This oxide, despite the fact that it has been studied for several decades [8, 35–42], remains a subject of extensive research as the scope of *ab initio* methods expands to include the treatment of defects [43] and their diffusion [44–46]. It is known that in metals the structure of defects [47] and atomic diffusion [48] are highly sensitive to magnetism. The experimental observation showing the effect of magnetic fluctuations on the thermal conductivity of UO_2 [15] suggests that other high-temperature transport properties may also be affected by the magnetic degrees of freedom.

The magnetic ground state of defect-free UO_2 has been extensively investigated both experimentally and theoretically [8, 35–39, 49]. However, a definitive verdict on the stability of the 3**k** magnetic ground state structure *and* the form of a low-energy spin excitation Hamiltonian suitable, for example, for spin-lattice dynamics simulations [17, 50, 51], still remains outstanding. Partly, the difficulty is associated with the fact that an *ab initio* treatment of oxide requires exploring the complexity of the energy landscape involving multiple local energy minima, which impedes applications of conventional energy minimization algorithms [52]. Also, it is necessary to take into account relativistic effects, giving rise to large SOC [40] and the emergence of multipolar spin interactions. Furthermore, it is necessary to determine the population of uranium f-orbitals, which result in the formation of orbital magnetic moments on uranium ions that are twice the magnitude of the spin moment [53]. Finally, magnetism is intimately linked to distortions of the underlying crystal structure, manifested in UO_2 via the Jahn-Teller (JT) instabilities [54], and non-collinear spin arrangement in the form of a 3**k**-ordered magnetic state. In this paper, we address the outstanding issues noted above using a consistent theoretical and methodological framework, aiming to uncover the ultimate quantum origin of the magnetic ground state in UO_2.

An important aspect of application of LSDA+U models to *ab initio* simulations of materials is the proper choice of values of the Coulomb repulsion and Hund's coupling parameters U and J. Owing to the difficulties inherent in evaluating the magnitude of these interactions, these quantities are generally treated as tunable parameters, and are chosen according to how well they reproduce some specific properties such as the band gap, the equilibrium volume, the magnetic moment or the formation energy [55]. In an attempt to improve the predictive capacity of LSDA+U models, several approaches have been proposed that aim to compute U and J without relying on phenomenological considerations [56–59]. Among them, the constrained random phase approxima-

tion (cRPA) allows one to take into account the effect of screening of the Coulomb interaction between correlated electrons and to estimate the magnitude of parameters U and J in the correlated subspace. The cRPA method has been successfully applied to a large variety of systems, and now represents a reliable and computationally viable method of obtaining accurate values of U and J [60–63]. In the analysis below, we apply this approach to computing U and J in the correlated f-subspace, in this way providing a solid reference for the values of these parameters in actinide compounds and allowing for a fully *ab initio*-based application of the LSDA+U model. In particular, the possibility to selectively compute U and J enables making an estimate of the role played by the prefactor in the parametrization of the LSDA+U scheme for predicting properties of non-collinear spin systems.

The manuscript is organized as follows. We start from deriving a non-collinear magnetic LSDA+U model, giving equations for the effective correcting one-electron potential and the double counting term, showing that the relevant formulae require only one parameter U as opposed to the difference $U - J$ found in the collinear version of the model. We then use cRPA to compute the value of U and compare the results with the available data. Subsequently, we address the question of stability of the non-collinear 3**k** magnetic structure and, by using an adiabatic occupation matrix approach, prove that the 3**k** structure represents the lowest energy configuration of UO$_2$ even in a perfect cubic lattice. Finally, we perform a detailed analysis of effective spin Hamiltonians and spin-spin interactions, concluding with the assessment of potential applications of the proposed methodology to computing high temperature properties, including simulations of atomic and magnetic dynamics.

II. A NON-COLLINEAR LSDA+U MODEL

The existing collinear LSDA+U model, which aims to provide an improved description of the electronic structure of materials characterized by strong electron correlations in spatially localized d and f shells, adds a correction term to the effective single particle electron potential [24, 25, 27]

$$V_{jl}^\sigma = \frac{\delta E_{\text{LSDA+U}}}{\delta \rho_{lj}^\sigma} = \frac{\delta E_{\text{LSDA}}}{\delta \rho_{lj}^\sigma} + (U-J)\left[\frac{1}{2}\delta_{jl} - \rho_{jl}^\sigma\right], \quad (1)$$

and a double counting correction to the total electronic energy [24]

$$E_{\text{LSDA+U}}^{dc} = \frac{(U-J)}{2}\sum_{\sigma,j,l}\rho_{jl}^\sigma\rho_{lj}^\sigma. \quad (2)$$

The latter is required to take into account the fact that a simple sum of single particle energies in a system of interacting electrons does not represent the correct contribution to the total energy, see e.g., Eq. (15) and Eq. (16)

of Ref. [64]. In Eq. (1) and Eq. (2), indexes j, l refer to orbitals associated with a lattice site, and σ is the spin index.

Eq. (1) and Eq. (2) were derived from a model tight-binding Hamiltonian [20, 65], where the on-site electron interaction terms have the form

$$\hat{\mathcal{H}} = \frac{U}{2}\sum_{l,l',\sigma}\hat{n}_{l,\sigma}\hat{n}_{l',-\sigma} + \frac{(U-J)}{2}\sum_{l,l',l\neq l',\sigma}\hat{n}_{l,\sigma}\hat{n}_{l',\sigma}. \quad (3)$$

It can be shown [26, 34] that the above Hamiltonian is identical to the Hamiltonian of the collinear Stoner model

$$\hat{\mathcal{H}} = \frac{U}{2}\left(\hat{N}^2 - \hat{N}\right) - \frac{J}{4}\left(\hat{N}^2 - 2\hat{N}\right) - \frac{J}{4}\hat{M}^2, \quad (4)$$

where $\hat{N}_\sigma = \sum_l \hat{n}_{l,\sigma}$, $\hat{N} = \hat{N}_\uparrow + \hat{N}_\downarrow$ and $\hat{M} = \hat{N}_\uparrow - \hat{N}_\downarrow$. Using the procedure outlined in Ref. [24], Eq. (1) and Eq. (2) can be derived by evaluating the expectation values of either Eq. (3) or Eq. (4).

Despite the relative success of the LSDA+U model [29], there are two points in the derivation that remain elusive. It is unclear to what extent the approximations associated with Hamiltonian (3) affect the form of Eq. (1) and Eq. (2), and also how to generalize these equations to non-collinear magnetic configurations, significant to applications [15, 17, 39]. The brief analysis given below addresses these two points.

First, we note that there is a major term missing in collinear Hamiltonians (3) and (4). This missing term has been identified in Ref. [34], and we show below that this term contributes to the LSDA+U correction, changing its form. Second, we note that the correction itself is not invariant in the extended space of spin and orbital indexes, a point that can be readily rectified using a suitable definition of the convolution of the full spin- and orbital-dependent electron density matrix.

To derive a non-collinear form of the LSDA+U model, we start by considering a model Hamiltonian, different from and more general than Eq. (3) or Eq. (4), and apply it to the parametrization of the LSDA+U equations, simplifying the full matrix representation of electron interactions. The treatment is based on a recent study by Coury *et al.* detailed in Ref. [34]. We find that application of the same methodology as what was followed in Ref. [24], to a more complete Hamiltonian [34], results in the LSDA+U equations that require only one parameter U as opposed to the two parameters U and J entering the formula derived in [24]. The general functional form of the LSDA+U correction remains the same.

An on-site Hamiltonian, describing interaction between electrons occupying orbitals i, j, k, l, is given by a sum of combinations of four creation and annihilation operators multiplied by a four-index matrix $V_{ij,lk}$:

$$\hat{\mathcal{H}} = \frac{1}{2}\sum_{i,j,k,l}\sum_{\sigma\xi}V_{ij,lk}\hat{c}_{i,\sigma}^\dagger\hat{c}_{j,\xi}^\dagger\hat{c}_{k,\xi}\hat{c}_{l,\sigma}. \quad (5)$$

Matrix V has $(2l+1)^4$ elements, which in the case of p (l=1) electrons amounts to 3^4=81 elements, and 5^4=625 elements in the case of d electrons. Symmetry constraints show that all the elements of $V_{ij,lk}$ can be parameterized using only two independent constants in the p-electron case, three constants in the d-electron case, and four in the f-electron case. In the p-electron cubic harmonic orbital case, using an analogy with the theory of isotropic elasticity [66], where the four-index matrix of elastic constants C_{ijkl} has the same symmetry as $V_{ij,lk}$, Hamiltonian (5) can be written *exactly* as [34]

$$\hat{\mathcal{H}} = \frac{1}{2}\left(U - \frac{J}{2}\right) : \hat{N}^2 : -\frac{J}{4} : \hat{\boldsymbol{M}}^2 : +\frac{J}{2}\sum_{i,j} : (\hat{n}_{ij})^2 : .$$
(6)

Here, $\hat{N} = \sum_{m,\sigma} \hat{c}^\dagger_{m,\sigma}\hat{c}_{m,\sigma}$ is the operator of the total number of electrons on a site, $\hat{n}_{kl} = \sum_\sigma \hat{c}^\dagger_{k,\sigma}\hat{c}_{l,\sigma}$, and

$$\hat{\mathbf{M}} = \sum_{m,\xi,\xi'} \hat{c}^\dagger_{m,\xi}\boldsymbol{\sigma}_{\xi\xi'}\hat{c}_{m,\xi'}$$

is the total vector magnetic moment operator associated with the site. In Eq. (6), :: denotes normal ordering of creation and annihilation operators. The normally ordered terms in Eq. (6), expressed using conventional notations, have the form

$$: \hat{N}^2 : = \hat{N}^2 - \hat{N},$$
$$: \hat{\boldsymbol{M}}^2 : = \hat{\boldsymbol{M}}^2 - 3\hat{N}.$$
$$: \hat{M}_z^2 : = \hat{M}_z^2 - \hat{N}.$$
$$: (\hat{n}_{kl})^2 : = \sum_{\sigma,\xi} \hat{c}^\dagger_{k,\sigma}\hat{c}^\dagger_{k,\xi}\hat{c}_{l,\xi}\hat{c}_{l,\sigma}.$$
(7)

The first two terms in Eq. (6) are identical to those entering Eq. (4), with the natural exception that now the magnetic moment operator is a vector quantity. Most significantly, in addition to the terms contained in Eq. (4), Hamiltonian (6) includes an extra third term, required by symmetry and absent in Eq. (4). This term is related to the orbital moment of electrons on a lattice site [34]. In the collinear approximation, where operator $\hat{\mathbf{M}}$ in Eq. (6) is replaced by its projection $\hat{M}_z = \hat{N}_\uparrow - \hat{N}_\downarrow$ on a quantization axis, and the third term in Eq. (6) is neglected, Hamiltonian Eq. (6) is identical to Eq. (4). We note that Hamiltonian (6) is exact in the sense that no procedure of "directional" averaging is involved in the transformation from Eq. (5) to Eq. (6).

We now follow the derivation given in Refs. [24, 25] and deduce the LSDA+U model from Hamiltonian (6). We identify the terms in Hamiltonian (6) that contain two creation and two annihilation operators acting on the same electronic state (m, σ). In the mean-field approximation, these terms provide contribution to the total energy proportional to $n^2_{m,\sigma}$ whereas their exact expectation value is proportional to $n_{m,\sigma}$. The LSDA+U model correction equals the difference between the exact and

mean-field expectation values of these terms, resulting in

$$E_{\text{LSDA}+\text{U}} - E_{\text{LSDA}} =$$
$$\left[\frac{1}{2}\left(U - \frac{J}{2}\right) - \frac{J}{4} + \frac{J}{2}\right]\sum_{m,\sigma}\left(n_{m,\sigma} - n^2_{m,\sigma}\right).$$
(8)

In the above expression, each term in square brackets corresponds to a respective term in Hamiltonian Eq. (6), and $n_{m\sigma}$ is the electron occupation number of an orbital state m with spin index σ.

We see that the terms in Eq. (8), which contain parameter J, cancel each other, and only the term proportional to parameter U remains. The sum of the first two terms in square brackets $(U - J/2)/2 - J/4 = (U - J)/2$ gives the coefficient found in the LSDA+U derivation given earlier [24], which was based on a collinear model Hamiltonian (4). The third term in square brackets in Eq. (8) stems from the last term in Hamiltonian (6), which is missing in the Hamiltonians [20, 65] used earlier. The full cancellation of the terms containing parameter J is perhaps not surprising, given the original form of the Hubbard Hamiltonian [67] that contains no J terms and is still able to generate a variety of magnetic solutions, originating solely from strong on-site electron correlations.

A general form of Eq. (8), invariant with respect to the choice of electronic orbitals and spin quantization axis, is now:

$$E_{\text{LSDA}+\text{U}} - E_{\text{LSDA}} = \frac{U}{2}\left[\text{Tr}\rho - \text{Tr}\rho^2\right]$$
$$= \frac{U}{2}\left[\sum_{m,\sigma}\rho^{\sigma\sigma}_{mm} - \sum_{m,\sigma;m',\sigma'}\rho^{\sigma\sigma'}_{mm'}\rho^{\sigma'\sigma}_{m'm}\right],$$
(9)

where ρ is the full orbital and spin-dependent one-electron density matrix.

In the collinear approximation, where the density matrix is assumed to be diagonal with respect to the subset of its spin indexes $\rho^{\sigma\sigma'}_{mm'} = \rho^\sigma_{mm'}\delta_{\sigma\sigma'}$, Eq. (9) is identical to equation (5) of Ref. [24]. In this limit, the only difference between equation (5) of Ref. [24] and Eq. (9) given above is the prefactor that, due to the presence of the third term in Hamiltonian (6), now equals $U/2$ as opposed to $(U - J)/2$ derived from Hamiltonian (3).

An invariant orbital- and spin-dependent noncollinear form of LSDA+U (1) and (2) is now:

$$V^{\sigma\sigma'}_{jl} = \frac{\delta E_{\text{LSDA}+\text{U}}}{\delta\rho^{\sigma\sigma'}_{lj}} = \frac{\delta E_{\text{LSDA}}}{\delta\rho^{\sigma\sigma'}_{lj}} + U\left[\frac{1}{2}\delta_{jl}\delta_{\sigma\sigma'} - \rho^{\sigma\sigma'}_{jl}\right],$$
(10)

and

$$E^{dc}_{\text{LSDA}+\text{U}} = \frac{U}{2}\sum_{\sigma,\sigma',j,l}\rho^{\sigma\sigma'}_{jl}\rho^{\sigma'\sigma}_{lj}.$$
(11)

The need to add the double counting term (11) to the total energy, evaluated using the conventional Kohn-Sham procedure, stems from the fact that the single-particle

electron potential (10) depends on the occupancy of electron orbitals through the term proportional to $\rho_{jl}^{\sigma\sigma'}$. It is this occupancy-dependent term in Eq. (10) that makes a simple sum of one-particle energies different from the total energy given by Eq. (9). The above equations show that, in addition to correcting the prefactor in the formula, a fully invariant LSDA+U construction requires convoluting the density matrix over the full set of its orbital and spin indexes, a point that was not addressed in earlier derivations [24, 25, 27].

Similarly to Eq. (8), the terms containing parameter J also cancel exactly if we perform the above derivation for the d-electron case [34]. The most direct way of carrying out the derivation is to start from equation (22) of Ref. [34] and note that in the d-electron case, all the terms containing parameter J can be expressed in terms of a renormalised parameter $J - 6\Delta J$, resulting in Eq. (9) given above, plus small terms proportional to ΔJ, which together amount to a small fraction of an electronvolt per atom and are normally neglected in applications [29]. This suggests that the single-parameter form of the LSDA+U correction given by Eq. (10) and Eq. (11) remains sufficiently accurate and applicable to d-electron orbitals, and other types of shells containing correlated electrons. Parameter U, according to the analysis given in [28, 60], is an effective quantity, characterizing the strength of electron-electron interactions, modified by effects of many-body self-screening. The significance of the above equations, in addition to the fact that they have been derived from a more accurate form of the on-site interaction Hamiltonian, is in that they can be used for treating non-collinear magnetic configurations.

III. *AB INITIO* METHODOLOGY

This section details the set of theoretical and methodological approaches adopted in this study. All the calculations were carried out using the Vienna *ab initio* simulation package (VASP) [68, 69], where the non-collinear extension of the Dudarev *et al.* LSDA+U scheme is implemented [70] with the full inclusion of relativistic effects (e.g., a full self-consistent treatment of spin-orbit coupling) [71]. A robust energy cut off up to 700 eV with the convergence precision of 10^{-6} eV was used in all the calculations, and the Brillouin zone was sampled using a $6{\times}6{\times}6$ k-point mesh. Atomic positions were optimized with the lattice parameters fixed at its observed value (a=5.469 Å) [72]. In what follows, we explore in considerable detail (A) the evaluation of interaction parameters U and J within the cRPA, (B) magnetically constrained density functional theory (DFT), (C) spin adiabatic occupation matrix approach to the calculation of magnetic energy landscape, (D) effective multipolar pseudospin Hamiltonian and exchange coupling, and (E) a strategy for estimating the strength of the SOC.

A. Constrained random phase approximation

Interaction parameters U and J were computed from first principles using the constrained random phase approximation [56]. In the cRPA, the Coulomb repulsion and Hund's coupling parameters U and J are derived from the matrix elements of U_{ijkl} written in terms of Wannier basis functions representing the correlated subspace (in this case, the uranium f states)

$$U_{ijkl} = \lim_{\omega \to 0} \iint d\mathbf{r}d\mathbf{r}' w_i^*(\mathbf{r}) w_j^*(\mathbf{r}') \mathcal{U}(\mathbf{r}, \mathbf{r}', \omega) w_k(\mathbf{r}) w_l(\mathbf{r}'). \tag{12}$$

More precisely, U and J are the average matrix elements U_{ijij} (intra- and inter-orbital interactions of the different spins) and U_{ijji} (inter-orbital interactions of the same spins), respectively. In Eq. (12), $\mathcal{U}$ is the partially screened interaction kernel, which is calculated by solving the Dyson-like equation

$$\mathcal{U}^{-1} = \mathcal{V}^{-1} - \chi^r, \tag{13}$$

where $\mathcal{V}$ is the bare (unscreened) interaction kernel and $\chi^r = \chi - \chi^t$ is the polarizability, excluding contributions from the "target" correlated f subspace, χ^t. Following this procedure, we have found U^{cRPA}=3.46 eV and J^{cRPA}=0.3 eV, corresponding to the effective interaction parameter $U_{\text{eff}}^{\text{cRPA}}$=3.16 eV. These values are expectedly smaller than those extracted from experimental estimates, adopted in previous LSDA+U studies of UO$_2$ [73]: U=4.5 eV and J=0.54 eV, U_{eff}=3.96 eV. In order to verify the role played by the prefactor $U/2$ entering Eq. (9) in the description of magnetic properties of UO$_2$, we have tested four different choices of interaction parameters, namely

1. U=3.16 eV (i.e. $U_{\text{eff}}^{\text{cRPA}}$)

2. U=3.46 eV (i.e. U^{cRPA})

3. U=3.96 eV (i.e. 'Expt.' U_{eff})

4. U=4.50 eV (i.e. 'Expt.' U)
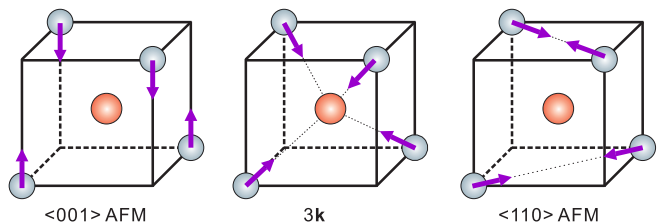
FIG. 1. Schematic plots of the $\langle 001 \rangle$-AFM, 3**k** (longitudinal) and $\langle 110 \rangle$-AFM non-collinear spin configurations considered in this study.

B. Magnetically constrained noncollinear DFT+U

To determine the non-collinear magnetic ground state of UO$_2$, we have minimized the total energy, treating it as a function of the direction of spin moments and using the magnetically constrained non-collinear DFT+U [11, 71, 74]. In particular, we have inspected spin rotations that transform the system from a characteristic non-collinear 3**k** state into collinear antiferromagnetically (AFM) ordered $\langle 001 \rangle$ and $\langle 110 \rangle$ configurations [39], illustrated in Fig. 1. A non-collinear 3**k** phase is described by three independent wave vectors and can be represented by a combination of three different phases: one longitudinal and two equivalent transverse configurations. To facilitate the construction of the canted magnetic energy landscape, we used the longitudinal 3**k** ordered magnetic structure shown in Fig. 1 as a starting configuration. The two other ordered AFM configurations, $\langle 001 \rangle$ and $\langle 110 \rangle$, belong to the 1**k** (one wave-vector) and 2**k** (two wave-vectors) categories, respectively.

The $\langle 001 \rangle$–3**k**–$\langle 110 \rangle$ magnetic structure transformation pathway can be defined by a concerted variation of angle θ on the four inequivalent uranium sites in the UO$_2$ magnetic unit cell [see Fig. 2(a) and (c)]. Constrained energy minimization as a function of θ along the transformation pathway is achieved by considering the energy penalty arising from constraining the direction of the spin magnetic moment, defined by the formula

$$E = E_0(\{\mathbf{M}_i\}) + \sum_i \gamma [\mathbf{M}_i - \mathbf{M}_i^0(\mathbf{M}_i^0 \cdot \mathbf{M}_i)]^2. \quad (14)$$

Here E_0 is the unconstrained DFT total energy, whereas the second term is a penalty contribution defined as a non-collinear directional constraint on the direction of local moments $\mathbf{M}_i$ with respect to an arbitrary set of unit vectors $\mathbf{M}_i^0$ on sites i. $\mathbf{M}_i$ is the magnetic moment computed by integrating over a Wigner-Seitz cell centered on atom i (the effective Wigner-Seitz radius is 1.588 Å for a U ion and 0.82 Å for an O ion). Parameter γ defines the magnitude of the energy penalty term, where by progressively increasing γ, functional (14) is driven to convergence towards the DFT total energy [74]. We used the value γ=10 that guarantees that the expectation value of the energy penalty term is lower than 10^{-5} eV.

C. Adiabatic spin occupation matrix approach

A known drawback of DFT+U approaches is the difficulty associated with finding the lowest energy state of a strongly correlated magnetic material. In most cases a DFT+U functional exhibits a multitude of local minima corresponding to a variety of spin and orbital occupancies in the correlated electronic subspace [39, 75–77]. The difficulty with finding a global minimum stems from the curvature of the energy surface as a function of orbital occupations [76]. In standard DFT calculations the
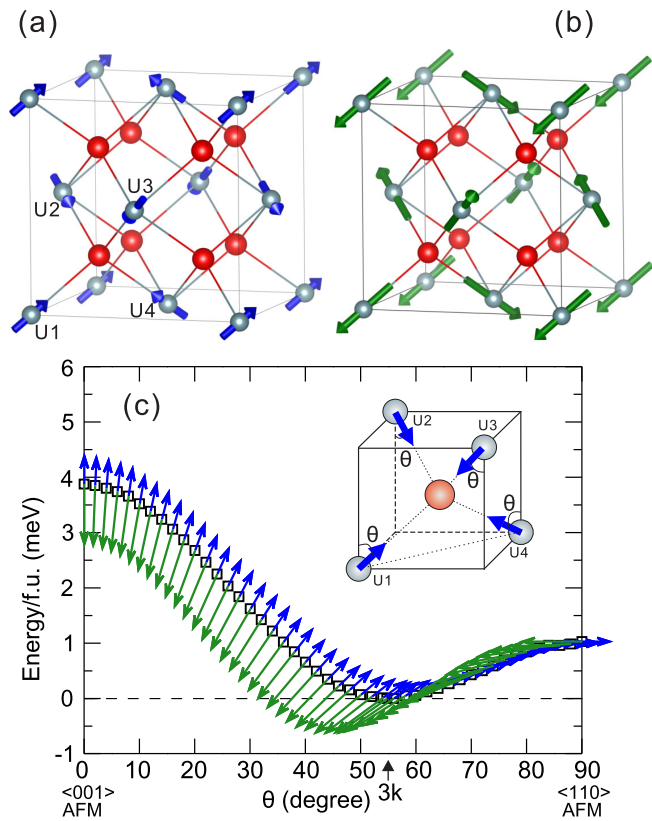

FIG. 2. Schematic view of (a) spin and (b) orbital moments in a 3**k** (longitudinal) magnetic unit cell of UO$_2$. Panel (c) shows the total energy as a function of the canting angle θ along the $\langle 001 \rangle$-AFM – 3**k** – $\langle 110 \rangle$-AFM transformation pathway. Blue and green arrows show the spin and orbital moments, respectively. The inset explains the definition of the spin canting angle θ adopted in our analysis.

energy surface is typically convex, but the global minimum might correspond to a physically unreasonable partial fractional orbital occupation, e.g. a metallic state of the material that in reality is an insulator. DFT+U corrects this by adding a term that penalizes fractional occupations, but this correction changes the curvature of the energy surface from convex to concave, unavoidably giving rise to many local minima [76]. Dorado and coworkers proposed to address this point by performing a search involving a large number of self-consistent calculations, each starting from different initial occupation matrices, and to select the outcome corresponding to the lowest total energy [75]. This procedure can be accelerated by adiabatically "turning on" the value of parameter U starting from the DFT limit $U = 0$ and gradually converging to the true ground state with integral orbital occupations [76]. The above issue is particularly pertinent to non-collinear spin systems, where small rotations of spin moments could give rise to many local minima, all lying in a few meV energy range.

Bearing in mind this aspect of energy minimization, we have combined the occupation matrix approach with
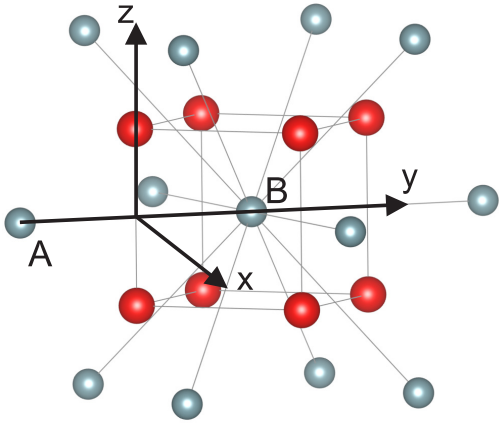
FIG. 3. Spin quantization axes x, y, and z and the geometry of the exchange-coupled pair for neighboring U^{4+} exchange ions. There are six inequivalent exchange-coupled pairs AB per a magnetic unit cell.

a gradual adiabatic change of the spin moment direction, using the magnetically constrained non-collinear DFT+U functional described in the previous subsection [11, 71, 74]. Starting from the 3**k**-type non-collinear spin ordered state of UO$_2$ [8, 39] shown in Fig. 2(a) we gradually changed the canting angle θ, moving adiabatically from the non-collinear 3**k** state to the energetically comparable AFM collinearly ordered $\langle 001 \rangle$ and $\langle 110 \rangle$ configurations shown in Fig. 2(c). At each canting step, we initialized the occupation matrix to the one obtained at the preceding step and performed fully self-consistent calculation. In this way, by gradually perturbing the wavefunction of the 3**k** state, we were able to construct a smooth total energy curve E(θ) as a function of the canting angle θ, shown in Fig. 2(c). The absence of cups and sudden jumps guarantees that this energy curve represents the lowest energy path linking the spin configurations considered here and that the 3**k** state is indeed the global minimum with respect to spin rotations. Probing other spin configurations (not shown here) confirmed this analysis and did result in finding spin configurations with lower total energies. We note that the orbital moment $\mathbf{m}_o$ remains antiparallel to the spin moment $\mathbf{m}_s$ everywhere on the transformation pathway, and the magnitudes of both moments are independent of the canting angle: $m_s \approx 1.5$ μ_B and $m_o \approx 3.2$ μ_B, see Fig. 2(b) and (c).

D. Effective pseudospin Hamiltonian and exchange interactions

To characterize magnetic properties of a material and to understand the origin of the specific spin ordered configuration that it adopts, it is necessary to quantify the dominant spin-spin interactions. For systems conserving the total spin moment, magnetic coupling parameters can be analyzed in terms of an effective Heisenberg

spin Hamiltonian involving conventional spin operators. In materials with strong spin-orbit coupling spin moments are not conserved and it is more appropriate to use pseudospin operators and pseudospin Hamiltonian [78] that are suitable for the treatment of multipolar interactions [79–81],

Within the pseudospin picture, spin and orbital degrees of freedom are not separated, and the operator set is formed by a unit multipole (tensor) operator $T_K^Q(J)$ [23, 82, 83] (here J is the angular moment, K the rank and $Q = -K, ..., K$), and in the most general form a multipolar exchange Hamiltonian can be written as [23, 83]

$$H = \sum_{ij} \sum_{KQ} C_{K_i K_j}^{Q_i Q_j} T_{K_i}^{Q_i} T_{K_j}^{Q_j}, \tag{15}$$

where i,j are the site indexes, $C_{K_i K_j}^{Q_i Q_j}$ are the coupling constants describing how the energy of the system changes as a result of variation of the two multipole moments $T_{K_i}^{Q_i}$ and $T_{K_j}^{Q_j}$.

UO$_2$ adopts non-collinear 3**k** ordered magnetic configuration and the two-electrons (f^2) ground state of a uranium ion is a Γ_5 triplet corresponding to the effective spin (pseudospin) $\tilde{S} = 1$ [21]. The Γ_5 ground state is associated with cooperative quadrupolar interactions that cannot be accounted for using a $S = 1/2$ Heisenberg model [9, 21, 23, 49, 84], but can be modeled by means of a suitable pseudospin Hamiltonian.

To compute spin-spin interactions in UO$_2$, we adopt the multipolar spin Hamiltonian derived by Mironov *et al.* [21], describing the superexchange interaction of neighboring U^{4+} ions in the $5f^2$ configuration. The general form of the Mironov Hamiltonian reads

$$H = A_0 + H_1 + H_2 + H_3 + H_4, \tag{16}$$

where A_0 is a spin-independent parameter, whereas the remaining terms accounts for various types of spin interactions, which can be written using conventional spin variables as

$$\begin{aligned} H_1 = {} & D[(S_A^z)^2 + (S_B^z)^2] \\ & + E[(S_A^x)^2 - (S_A^y)^2 + (S_B^x)^2 - (S_B^y)^2] \end{aligned} \tag{17}$$

$$H_2 = J_x S_A^x S_B^x + J_y S_A^y S_B^y + J_z S_A^z S_B^z, \tag{18}$$

$$\begin{aligned} H_3 = {} & j_1 S_A^x S_B^x [(S_A^z)^2 + (S_B^z)^2] + 2j_1 S_A^y S_B^y S_A^z S_B^z \\ & + j_2 S_A^y S_B^y [(S_A^z)^2 + (S_B^z)^2] + 2j_2 S_A^x S_B^x S_A^z S_B^z \end{aligned} \tag{19}$$

$$\begin{aligned} H_4 = {} & q_1 O_A^{(1)} O_B^{(1)} + q_2 O_A^{(2)} O_B^{(2)} + q_3 O_A^{(3)} O_B^{(3)} \\ & + q_4 [O_A^{(1)} O_B^{(2)} + O_A^{(2)} O_B^{(1)}]. \end{aligned} \tag{20}$$

Here, H_1 is a single-spin term, quadratic in the spin components and accounting for the zero field splitting (ZFS) dipolar interactions; the ZFS parameters D and E describe the axial and transversal components of magnetic dipole-dipole (DD) interaction, respectively. H_2 is bilinear in spins (and isotropic under rotations) and describes

spin exchange interactions (sometimes called the Heisenberg exchange), parameterized by J_x, J_y and J_z. The term H_3 describes four-spin exchange interactions with j as the corresponding coupling constant. Finally, H_4 accounts for biquadratic quadrupole-quadrupole (QQ) interactions, where $O_{A,B}^{(n)}$ are the components of the quadrupole operator, specifically:

$$O_k^{(1)} = (S_k^z)^2 - S(S+1)/3 \qquad (21)$$

$$O_k^{(2)} = (S_k^x)^2 - (S_k^y)^2 \qquad (22)$$

$$O_k^{(3)} = S_k^x S_k^y + S_k^y S_k^x, \qquad (23)$$

where $k =$A, B. Labels A and B refer to the interacting nearest neighbour Uranium ions, see Fig. 3 for details. There are four inequivalent sites in a magnetic unit cell of UO$_2$ [U1–U4, see Fig. 2(a)] producing six inequivalent nearest neighbor AB pairs: A=U1, B=U2; A=U1, B=U3; A=U1, B=U4; A=U2, B=U3; A=U2, B=U4; A=U3, B=U4. S_A and S_B are the two spins forming a distinct inequivalent AB pair, and x, y, and z are the local quantization axes illustrated in Fig. 3. Cartesian components of spins S_A and S_B in the local quantization axis representation are given in the Supplementary Materials [85].

The *ab initio* evaluation of the above superexchange parameters is a difficult task [22, 23]. First, we would like to note that depending on a specific definition of the tensor operators, slightly different forms of superexchange coupling can be found in literature [9, 21, 23, 84], impeding accurate quantitative comparison with existing data.

In the formulation of the effective pseudospin Hamiltonian we have followed the procedure by Mironov [21]. To estimate the magnitude of effective magnetic interactions, Mironov *et al.* used a second-order perturbation approach, using free-ion and cubic crystal-field parameters and limiting the interaction to the two nearest-neighbor U atoms only. In our analysis, we estimate the dominant exchange couplings by means of a controlled fitting procedure, involving the mapping of $\Delta E(\theta)$ onto DFT+U+SOC total energies to Eq. (16). To achieve this, we have rewritten the four terms entering Eq. (16) as functions of the canting angle θ, replacing components of spins by their explicit expressions in terms of local Cartesian components and arriving at the total magnetic energy expressed as a function of θ. After some algebra, we find that $\Delta E(\theta)$ has the form

$$\Delta E(\theta) = B_0 + B_1 \cos(\theta) + B_2 \cos(2\theta) + B_3 \cos(3\theta)$$
$$+ B_4 \cos(4\theta) + C_1 \sin(\theta) + C_2 \sin(2\theta) + C_4 \sin(4\theta), \qquad (24)$$

where the coefficients are given in terms of the eleven superexchange parameters entering the Mironov Hamiltonian (D, E, J_x, J_y, J_z, j_1, j_2, q_1, q_2, q_3, and q_4):

$$B_0 = 6D + 3/2J_x + 3/2J_y + 3J_z + 3j_1 + 3j_2 \qquad (25)$$
$$+ 3q_1 + 3/2q_2 + 3q_4 - 2q_1 S + (4D - 2E$$
$$- 2j_1 - 2j_2 - 3/2J_x - 5/2J_y + 2J_z$$
$$+ 14/3q_1 - 4q_2 - 4q_3 - q_4)S^2 + 2/3q_4 S^3$$
$$+ 1/24(11q_1 + 42q_2 + 33q_3 + 4q_4$$
$$- 42j_1 - 42j_2)S^4$$

$$B_1 = (4D + 2J_z + 2j_1 + 2j_2 + 4q_1 + 2q_4)S \qquad (26)$$
$$- 4/3q_1 S^2 - (j_1 + j_2 - 5/3q_1 + 3q_4)S^3$$

$$B_2 = (2E - 1/2J_x + 1/2J_y + q_4)S^2 - 2/3q_4 S^3 \qquad (27)$$
$$+ (j_1 + j_2 + 1/2q_1 - q_2 + 3/2q_3 - 2/3q_4)S^4$$

$$B_3 = (j_1 + j_2 + q_1 + 3q_4)S^3 \qquad (28)$$

$$B_4 = 1/8(6j_1 + 6j_2 + 3q_1 - 6q_2 + 9q_3 + 4q_4)S^4 \qquad (29)$$

$$C_1 = (4D + 2j_1 + 2j_2 + 2J_z + 4q_1 + 2q_4)\sqrt{2}S \qquad (30)$$
$$- 4\sqrt{2}/3q_1 S^2 + \sqrt{2}/6(q_1 - 15j_1 - 15j_2)S^3$$

$$C_2 = (-4E + J_x - J_y - 2q_4)\sqrt{2}S^2 \qquad (31)$$
$$+ 4\sqrt{2}/3q_4 S^3 + \sqrt{2}/3q_4 S^4$$

$$C_4 = \sqrt{2}/2q_4 S^4. \qquad (32)$$

E. Calculation of the spin-orbit coupling strength

We conclude the methodological section with an estimate of the strength of SOC in UO$_2$. To produce this estimate, we relate the relativistic total energies obtained from first principles calculations to the relativistic atomic Hamiltonian for f orbitals:

$$H_{SOC} = \lambda \, \mathbf{L} \cdot \mathbf{S}, \qquad (33)$$

where λ defines the SOC strength. By using the 14 f ($l = 3$) spinors as a basis in the following order: $|xyz, \uparrow \rangle$, $|x(5x^2 - 3r^2), \uparrow\rangle$, $|y(5y^2 - 3r^2), \uparrow\rangle$, $|z(5z^2 - 3r^2), \uparrow\rangle$, $|x(y^2 - z^2), \uparrow\rangle$, $|y(z^2 - x^2), \uparrow\rangle$, $|z(x^2 - y^2), \uparrow\rangle$ (and the corresponding $\uparrow \Rightarrow \downarrow$ spinors), the atomic Hamiltonian H_{SOC} can be written as a (14×14) matrix, see Eq. (34) below [86].

The diagonalization of matrix (34) yields the following eigenvalues $-\lambda$, $-\lambda$, $-\lambda$, $-\lambda$, $-\lambda$, $-\lambda$, $3\lambda/4$, $3\lambda/4$, $3\lambda/4$, $3\lambda/4$, $3\lambda/4$, $3\lambda/4$, $3\lambda/4$, $3\lambda/4$. From the eigenvalues of the SOC Hamiltonian, it is possible to extract the contribution to the total energy from the SOC effects, ΔE_{soc}, by considering either the SOC-induced splitting ($\frac{7}{4}\lambda$) or the energy contribution arising from the occupied states. We have followed the latter route, as in this case a suitable mapping can be constructed between the atomic limit (H_{SOC}) and realistic *ab initio* calculations. Specifically, considering that U^{4+} ions in UO$_2$ are in the $5f^2$ electronic configuration, the two electrons occupy the lowest two eigenvalues ($-\lambda$) resulting

in $\Delta E_{\text{soc}} = -2\lambda$. An estimate of ΔE_{soc} can be obtained from the DFT total energy difference between a relativistic (with SOC) and a non-relativistic calculation (no SOC), i.e., $\Delta E_{\text{soc}} = E_{\text{SOC}} - E_{\text{noSOC}}$. To exclude the spurious energy contributions arising from the difference between electronic ground states, this estimate was obtained using the metallic solutions with $U = 0$ and the $\mathbf{3k}$ spin ordered configuration (in fact

DFT+U, unlike DFT+U+SOC, delivers a metallic solution). We should mention that in the metallic solution without any U the values of the spin and orbital moments are greatly reduced with respect to the those obtained for the DFT+U+SOC ground state, specifically $m_s \approx 1$ μ_B and $m_o \approx 1.5$ μ_B. Within this scheme we find that $\Delta E_{\text{soc}} = -2.98$ eV per uranium ion, corresponding to $\lambda = -\Delta E_{\text{soc}}/2 = 1.49$ eV.

$$H_{\text{SOC}} = \frac{\lambda}{4} \begin{pmatrix} 0 & 0 & 0 & 0 & 0 & 0 & 2i & 0 & 0 & 0 & 0 & 2i & 2 & 0 \\ 0 & 0 & 3i/2 & 0 & 0 & it & 0 & 0 & 0 & 0 & -3/2 & 0 & 0 & t \\ 0 & -3i/2 & 0 & 0 & it & 0 & 0 & 0 & 0 & 0 & 3i/2 & 0 & 0 & it \\ 0 & 0 & 0 & 0 & 0 & 0 & 0 & 0 & 3/2 & -3i/2 & 0 & t & it & 0 \\ 0 & 0 & -it & 0 & 0 & -i/2 & 0 & -2i & 0 & 0 & -t & 0 & 0 & 1/2 \\ 0 & -it & 0 & 0 & i/2 & 0 & 0 & -2 & 0 & 0 & -it & 0 & 0 & -i/2 \\ -2i & 0 & 0 & 0 & 0 & 0 & 0 & 0 & -t & -it & 0 & -1/2 & i/2 & 0 \\ 0 & 0 & 0 & 0 & 2i & -2 & 0 & 0 & 0 & 0 & 0 & 0 & 0 & -2i \\ 0 & 0 & 0 & 3/2 & 0 & 0 & -t & 0 & 0 & -3i/2 & 0 & 0 & -it & 0 \\ 0 & 0 & 0 & 3i/2 & 0 & 0 & it & 0 & 3i/2 & 0 & 0 & -it & 0 & 0 \\ 0 & -3/2 & -3i/2 & 0 & -t & it & 0 & 0 & 0 & 0 & 0 & 0 & 0 & 0 \\ -2i & 0 & 0 & t & 0 & 0 & -1/2 & 0 & 0 & it & 0 & 0 & i/2 & 0 \\ 2 & 0 & 0 & -it & 0 & 0 & -i/2 & 0 & it & 0 & 0 & -i/2 & 0 & 0 \\ 0 & t & -it & 0 & 1/2 & i/2 & 0 & 2i & 0 & 0 & 0 & 0 & 0 & 0 \end{pmatrix}, \quad t = \sqrt{15}/2 \tag{34}$$

Further support for this large value of λ comes from an approximate scaling of the magnitude of SOC at atomic level, where it is known that the SOC parameter λ is proportional to Z^4, where Z is the atomic number. By rescaling the SOC strength of iridium (0.5 eV) [87] with the relative nuclear charge of Ir (Z_{Ir}) and U (Z_{U}) we find

$$\lambda_{\text{U}} \approx \lambda_{\text{Ir}}(Z_{\text{U}}/Z_{\text{Ir}})^4 = 0.5 \text{ eV} \times (92/77)^4 = 1.02 \text{ eV},$$

confirming the very large value of SOC parameter in uranium.

IV. RESULTS AND DISCUSSION

The strong SOC in UO_2 is responsible for the formation of a Γ_5 triplet described by an effective pseudospin $\tilde{S} = 1$ [21] state where the spin and orbital moments are ordered in a $\mathbf{3k}$ magnetic structure [8, 88], see Fig. 2(a) and (b). Moreover, the various types of (multipolar) superexchange interactions acting in the $\mathbf{3k}$ magnetic configuration are coupled with the cooperative Jahn-Teller (JT) effect, manifested by a distortion of the oxygen cage around the U^{4+} ions [9, 16, 36, 83]. The computational verification of these experimental observations and their interpretation on a quantum level is a difficult task due to a variety of factors: (i) magnetic non-collinearity, (ii) self-interaction acting in the U-f manifold, and (iii) existence of multiple local minima in a narrow energy interval [38, 39, 75]. As was noted above, a combination of

fully relativistic and magnetically constrained DFT+U with adiabatic evolution of the occupation matrix is able to predict the ground state of UO_2 [Fig. 2(c)] and should help decipher the subtleties of electronic and magnetic effects in UO_2.

To gain insight into the nature of magnetic interactions, we compute the magnetic energy curves similar to the one shown in Fig. 2, but this time performing the calculations for several different values of prefactor U used in the DFT+U formalism. The curves shown in Fig. 4 suggest that the non-collinear $\mathbf{3k}$ ordering remains the lowest energy state for any value of U, but the energy difference between the $\mathbf{3k}$ phase and the competing AFM collinear phases $\langle 001 \rangle$ and $\langle 110 \rangle$, illustrated in Fig. 1, depends sensitively on the choice of U. As the value of U increases, the relative stability of the $\mathbf{3k}$ state decreases, and it becomes progressively less energetically costly to rotate the spins. This implies that the value of the magnetic exchange interactions is also sensitive to the choice of U. We shall discuss this later in the section.

The role of parameter U is also reflected in the fundamental electronic and magnetic properties of the $\mathbf{3k}$ ground state. Table I gives values of the spin moment m_s, the orbital moment m_o, and the insulating gap E_g calculated for U=3.16, 3.46, 3.96 and 4.50 eV. While the moments are only marginally affected by the choice of U (and all of them compare well with the observed total moment of 1.74 μ_B [90]), the band gap varies significantly from 1.91 eV to 2.78 eV. The best agreement
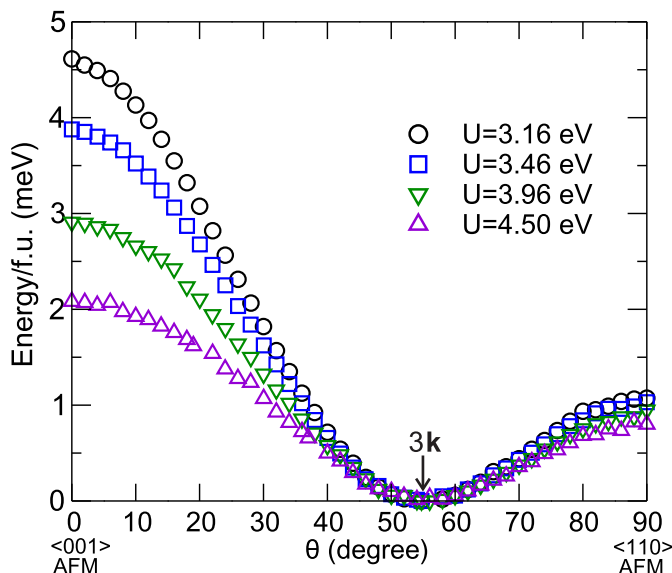
FIG. 4. Total energy as a function of the canting angle θ computed for several different values of parameter U.

TABLE I. Values of spin (m_s), orbital (m_o), and total (m_t) moments (in μ_B units) and the electronic band gap E_g (in eVs) corresponding to several different values of parameter U (in eVs). The experimentally observed band gap and the local total magnetic moment on Uranium ions are ≈ 2.0 eV [89] and 1.74 μ_B [90], respectively.

	$U=3.16$	$U=3.46$	$U=3.96$	$U=4.50$
m_s	-1.52	-1.53	-1.54	-1.54
m_o	3.18	3.19	3.21	3.22
m_t	1.66	1.66	1.67	1.68
E_g	1.91	2.11	2.44	2.78

with experiment ($E_g \approx 2.0$ eV [89]) is found for the relatively small U, in agreement with the first principles estimate of the Coulomb interaction parameters based on the cRPA (see Sec. III A), and also in agreement with the results of the recent fitting analysis [41]. We also note that even though the value of parameter J in UO$_2$ is not very large, 0.3 eV, its effect on the band gap is not negligible, and is of the order of 10% (E_g=1.91 eV for $U = U^{\mathrm{cRPA}} - J^{\mathrm{cRPA}}$=3.16 eV and E_g=2.11 eV for $U = U^{\mathrm{cRPA}}$=3.46 eV, both fairly close to the observed band gap of approximately 2.0 eV).

Next, we examine the quantum mechanism responsible for the onset of magnetic 3**k** ordering. We remind the reader that in a Jahn-Teller-active material with strong SOC, the Jahn-Teller (JT) instability and exchange interactions are antagonists since the JT effect tends to stabilize states with quenched orbital momentum whereas SOC tends to maximize the orbital momentum [91]. This conclusion is generally valid if the crystal field is large, but in UO$_2$ the strength of SOC is very large (≈ 1.5 eV according to the estimate above) exceeding the energy scale of crystal-field excitations (150-180 meV [88]), and

therefore the spin-orbit interaction can be safely considered as the dominant energy scale and the leading factor stabilizing the 3**k** state. To verify this hypothesis, we have calculated the total energy of 1**k**, 2**k**, and 3**k** magnetically ordered states as a function of strength of the JT effect, switching it on and off. In the on mode we have adopted the self-consistent value of displacement in the oxygen cage, 0.003 Å, and examined two values of SOC, the full SOC strength $\lambda = 1.49$ eV and half SOC strength $\lambda = 0.75$ eV. The data, given in Table II, show that the JT effect has virtually no influence on the relative energies of magnetic configurations. The energy landscape and the energy difference between the 3**k**, 2**k** and 1**k** states remain essentially unchanged. This unambiguously demonstrates that the JT effect is not the mechanism that drives the system towards the 3**k** ground state [92]. In contrast, rescaling the SOC strength to half the original value ($\lambda = 0.75$ eV) causes a huge energy change favourable for both the $\langle 001 \rangle$-AFM and $\langle 110 \rangle$-AFM configurations, the latter becoming the most favorable one by more than 11 meV/f.u. This provides a clear indication that SOC is the major driving force responsible for the stabilization of the 3**k** state; reducing SOC strength leads to the over-stabilization of collinear magnetic structures.

TABLE II. Total energies (in meV/f.u.) of the $\langle 001 \rangle$-AFM, $\langle 110 \rangle$-AFM and 3**k** phases as a function of the Janh-Teller distortion and the strength of SOC, rescaled to a half of the self-consistent value $\lambda = 1.49$ eV. All the data given in the table were computed for U=3.46 eV.

JT effect	$\langle 001 \rangle$-AFM	3**k**	$\langle 110 \rangle$-AFM
undistorted	3.86	0.00	1.01
JT distorted	3.87	0.00	1.03
SOC strength	$\langle 001 \rangle$-AFM	3**k**	$\langle 110 \rangle$-AFM
0.5λ	-8.78	0.00	-11.28
λ	3.87	0.00	1.03

To discern how SOC stabilizes the 3**k** ordering of moments, we have explored the differences between electronic and magnetic properties of these three phases. Surprisingly, there are only marginal changes in the magnitude of spin and orbital moments (see Table III), in the band structure (see Fig. 5), as well as in the occupation numbers of states in the f manifold (see Table IV). A closer inspection of the band structure shows that even though the overall bonding picture in all the three magnetically ordered configurations is almost identical (including the size of the band gap), the f-manifold in the 3**k** phase exhibits larger SOC-induced splitting, which causes a change in the band topology.

To better understand the significance of this change in the topology of band structure, in Fig. 6 we plot charge-density isosurfaces for the occupied f orbitals in the energy interval (-2, 0) eV, projected onto a (110) plane containing both uranium and oxygen ions. The results show that the 3**k** configuration is the only spin arrangement ex-

TABLE III. Magnetic moments of uranium ions computed for the $\langle 001 \rangle$-AFM, $\langle 110 \rangle$-AFM and 3$\mathbf{k}$ magnetic configurations. All the values were computed assuming U=3.46 eV.

	$\langle 001 \rangle$-AFM	$\langle 110 \rangle$-AFM	3$\mathbf{k}$
m_s	-1.55	-1.51	-1.53
m_o	3.26	3.24	3.19
m_t	1.70	1.73	1.66
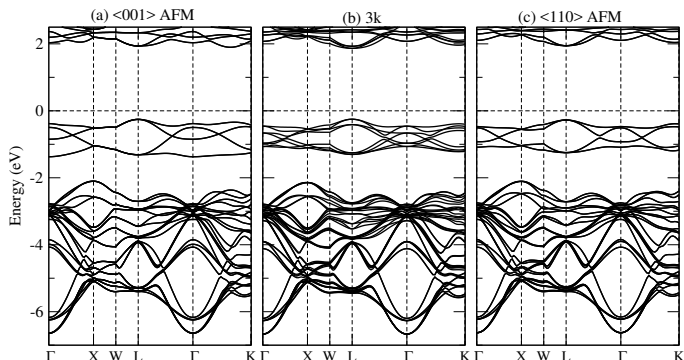
FIG. 5. Band structures of UO$_2$ computed for the $\langle 001 \rangle$-AFM, 3$\mathbf{k}$ and $\langle 110 \rangle$-AFM ordered configurations assuming U=3.46 eV.

TABLE IV. Eigenvalues of the 14×14 occupation matrix of the f manifold of uranium ions in UO$_2$ computed for the $\langle 001 \rangle$-AFM, 3$\mathbf{k}$ and $\langle 110 \rangle$-AFM spin configurations. All the values were computed for U=3.46 eV.

$\langle 001 \rangle$-AFM	3$\mathbf{k}$	$\langle 110 \rangle$-AFM
0.0268	0.0271	0.0273
0.0274	0.0282	0.0275
0.0296	0.0288	0.0296
0.0316	0.0341	0.0333
0.0348	0.0356	0.0359
0.0390	0.0365	0.0362
0.0397	0.0366	0.0375
0.0398	0.0384	0.0391
0.0454	0.0488	0.0477
0.0501	0.0508	0.0513
0.1233	0.1238	0.1238
0.1393	0.1407	0.1404
0.9852	0.9846	0.9846
0.9888	0.9858	0.9860

hibiting a visible orbital anisotropy at the uranium sites, associated with the canted ordering of f orbitals. The f-orbitals are rotated towards the nearest oxygen sites, following the same chessboard configuration of the 3$\mathbf{k}$ spin ordering as that shown in Fig. 2(a) and (b). Remarkably, the effect of SOC, critical to the stabilization of the 3$\mathbf{k}$ phase, is manifested primarily in the shape of f-orbitals rather than in the total orbital occupation, as illustrated in Table IV. The energy required to stabilize the 3$\mathbf{k}$ state over the $\langle 001 \rangle$-AFM and $\langle 110 \rangle$-AFM configurations is gained from a SOC-induced rotation of occupancies of particular orbitals, which follows the rotation of the local spin moments and enables constructive interaction with the oxygen electronic states.

Having established the DFT+U^{cRPA}+SOC as a suitable theory for the ground state electronic properties of UO$_2$, which highlights the significance of SOC in this compound, we are now ready to proceed to the analysis of the superexchange spin interaction mechanisms, to deduce information about the quantum origin of the 3$\mathbf{k}$ state. As we noted in the computational section, this can be done by fitting the magnetic energy computed using *ab initio* methods, to the multipolar Hamiltonian (24). The presence of eleven parameters in the expression for the multipolar Hamiltonian clearly poses a well known problem for the multi-parameter fitting procedure [93]. To handle this complication, we rely on the work by Mironov *et al.* [21] that can be summarized as follows. First, we note that using the values of parameters evaluated by Mironov (collected in Table V) in the pseudospin Hamiltonian, already leads to an overall fairly good account of the first principles magnetic energy, as illustrated graphi-

cally in Fig. 7. Even though the two curves do not match well, Mironov's parameters predict the correct minimum, located at the 3$\mathbf{k}$ position, suggesting that all the relevant magnetic coupling terms are included in the theoretical scheme. However, Mironov's parameters deliver a curve that varies over a significantly narrower energy interval than the curve derived from the first principles data, and as a result the relative stability of the 3$\mathbf{k}$ state with respect to the collinear 1$\mathbf{k}$ and 2$\mathbf{k}$ states is underestimated by about 50%.

The exchange parameters in Mironov's model fall into four different categories, namely (i) single-spin parameters D and E, (ii) bilinear parameters J_x, J_y and J_z, (iii) parameters describing the four-spin terms j_1 and j_2 and (iv) parameters of biquadratic interactions q_1, q_2, q_3, and q_4. The accuracy of Mironov's approach can be improved by noting that, according to the calculations by Savrasov and coworkers, the strength of quadrupolar (QQ) interactions computed by Mironov is underestimated by an order of magnitude [23]. Following this argument, we have fitted $\Delta E(\theta)$ by varying the two largest quadrupolar terms (q_1, q_2) only, and keeping all the other superexchange parameters fixed to the original Mironov's values. The resulting curve is in excellent agreement with first principles energies (χ^2_R=0.9989, see Fig. 7), and this improvement is associated with a very large increase of the magnitude of the quadrupolar terms, approximately by an order of magnitude (q_1+q_2)/2=4.56 meV, see Table V. However, this is in very good agreement with the earlier DFT+U data (3.1 meV [23]) and the values extracted from experimental spin-wave spectra (1.9 meV) [49]. As expected, the values of q_1 and q_2 are sensitive to the choice of parameter U, see TableVI. The strength of the QQ interaction increases as a function of U, this in particular applies to the the anisotropic biquadratic interaction q_2. Nevertheless, the resulting values do not depend on the Jahn-Teller distortions; using the undistorted cubic
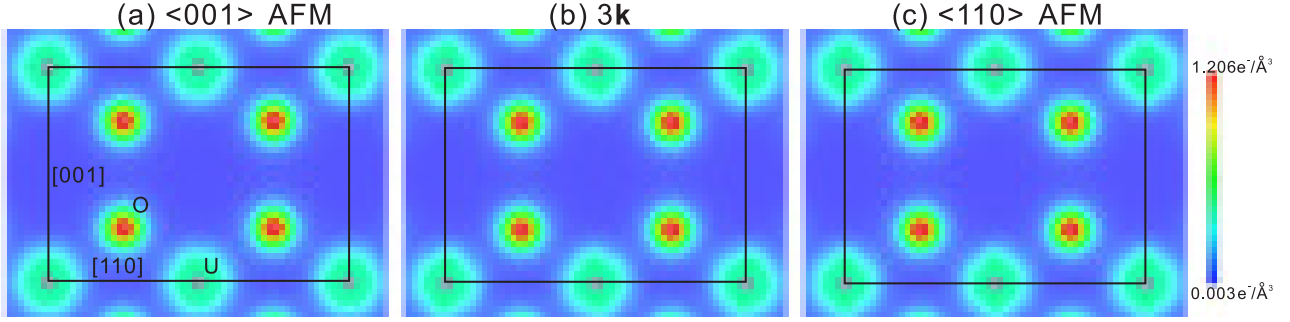
FIG. 6. Charge densities of UO$_2$ in a (110) plane computed for the $\langle 001 \rangle$-AFM, 3**k** and $\langle 110 \rangle$-AFM spin ordered configurations. All the three plots were computed assuming that U=3.46 eV.

phase one obtains essentially the the same values of parameters, further demonstrating the fairly negligible role played by the JT effect in stabilizing the 3**k** non-collinear state.
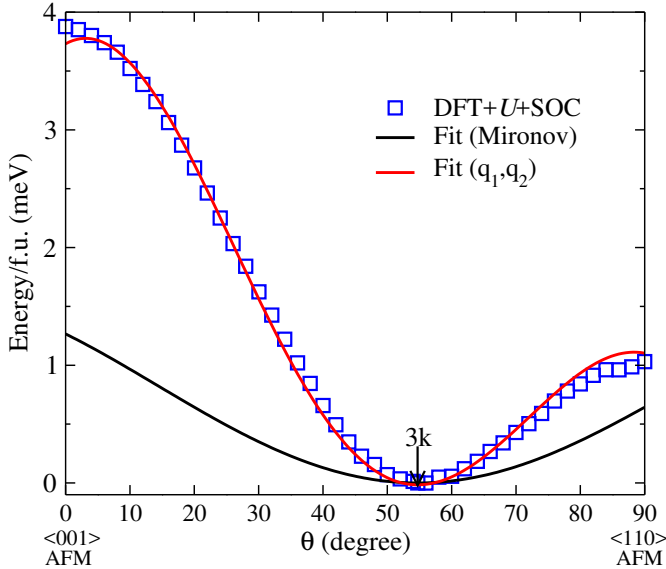

FIG. 7. Comparison between the calculated (DFT+U^{cRPA}+SOC) and fitted (out fit using Mironov's parameters) magnetic canting energies $\Delta E(\theta)$. In our fit we employed an extension of the Mironov model to all the U-U interactions and optimized the fit with respect to the dominant quadrupolar terms q_1 and q_2, by keeping all the other terms fixed to the corresponding values obtained by Mironov [21] (see Table V).

We conclude the discussion of magnetic properties of UO$_2$ by analyzing the individual contributions of various types of superexchange mechanisms to the stabilization of the 3**k** state. As was noted in the section on computational methods, the total magnetic Hamiltonian is expressed as the sum of four terms, each corresponding to a specific type of superexchange interaction: H_1 accounts for the DD interaction [Eq. (17)], H_2 describes the bilinear exchange [Eq. (18)], H_3 represents the four-
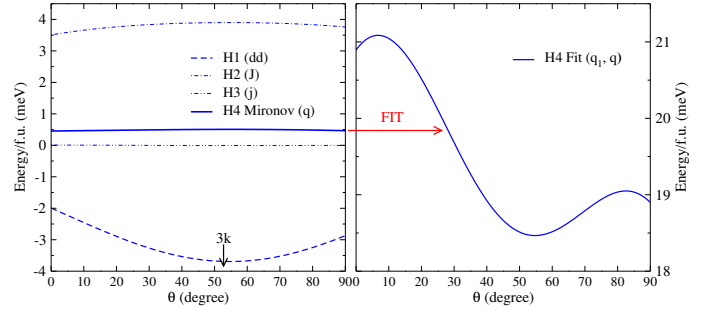

FIG. 8. Decomposition of the magnetic energy $\Delta E(\theta)$ into four components H_1 [DD interaction, D & E, Eq. (17)], H_2 [bilinear exchange, J's, Eq. (17)], H_3 [four-spin exchange, j's, Eq. (19)], and H_4 [quadrupolar, q's, Eq.(20)]. The right panel show the difference between the quadrupolar term derived directly from Mironov's data and our fitted curve.

spin exchange [Eq. (19)], and finally H_4 takes care of the quadrupolar coupling [Eq. (20)]. The data, summarized in Fig. 8, clearly show that the formation of the 3**k** state occurs as a result of a concerted action of DD and octupolar interactions. The contributions of bilinear exchanges (H_2, J's) and four spin exchanges (H_3, j's) are essentially independent of the canting angle, resulting in the rather flat curves. On the other hand, DD interactions have a quadratic-like trend with a marked minimum at 3**k** and the fit-corrected quadrupolar term (the right panel of Fig. 8) not only has a minimum at 3**k**, but also correctly describes the energy pathway from the 3**k** to the 1**k** and 2**k** states, following the trend exhibited by the first principles energies (see Fig. 7).

Based on the above results, we can conclude that the onset of the 3**k** state in UO$_2$ is driven, at the quantum level, by a concerted action of DD and QQ spin interactions. These interactions are active in the undistorted and JT-distorted crystal lattices, clearly indicating that, despite the existing coupling between the spin and lattice degrees of freedom, the JT instabilities do not contribute to the formation of the non-collinear 3**k** ordering, which is present also in the undistorted cubic phase.

TABLE V. Magnetic coupling parameters (meV) estimated by Mironov [21] shown together with the fitted values of the dominant QQ terms obtained by mapping the DFT+U^{cRPA}+SOC energies onto the extended Mironov's Hamiltonian. χ_R^2 serves as an indication of the quality of the fit in terms of the reduced chi-squared test.

	D	E	J_x	J_y	J_z	j_1	j_2	q_1	q_2	q_3	q_4	χ_R^2
Mironov [21]	-0.57	0.64	1.82	2.74	2.33	-0.04	0.05	0.22	0.32	0.07	-0.02	
Fit (QQ)								$\underline{7.18}$	$\underline{1.94}$			0.9989

TABLE VI. Fitted quadrupolar parameters q_1 and q_2 (and their average, in meV) as a function of U.

	q_1	q_2	$(q_1+q_2)/2$
$U = 3.16$ eV	6.55	0.36	3.46
$U = 3.46$ eV	7.18	1.94	4.56
$U = 3.96$ eV	7.64	3.77	5.71
$U = 4.50$ eV	7.81	5.19	6.50

TABLE VII. Summary of parameters controlling the magnitude of the relevant energy scales in UO_2: U & J (from cRPA), the SOC strength parameter λ, the QQ exchange (from fitting to the spin canting *ab initio* data) and DD exchange (from Mironov [21]).

U^{cRPA}	J^{cRPA}	λ	QQ	DD
3.46 eV	0.3 eV	1.49 eV	3.46 meV	≈ 0.6 meV

V. SUMMARY AND CONCLUSIONS

In conclusion, in this study we have addressed the issue of parametrization of the LSDA+U approximation for non-collinear spin systems and explained the origin of the canted 3**k** state in UO_2 by combining an array of advanced computational techniques including the constrained random phase approximation to compute the Coulomb repulsion parameter U and the Hund's coupling parameter J, thus rendering the LSDA+U+SOC fully *ab initio*, magnetic constrains to study the dependence of the total energy on the direction of the spin moment, adiabatic propagation of the occupation matrix to avoid the multiple minima problem in constructing the accurate magnetic energy landscape, and two different effective Hamiltonians to extract from the *ab initio* data the value of the spin-orbit interaction λ (achieved using an atomic-like relativistic Hamiltonian for f orbitals) and the quadrupole-quadrupole exchange interactions (using an effective pseudospin Hamiltonian).

The outcome of our study is threefold. First, we have derived an invariant orbital- and spin-dependent formalism for the LASD+U model for non-collinear spins that involves a spin and orbital convolution of the density matrix, and have shown that, unlike in collinear LSDA+U, the non-collinear LSDA+U potential and double counting correction depend on one parameter U only, and is independent on Hund's coupling parameter J. Second, our data suggest that the spin-orbit interaction parameter in UO_2 is as large as 1.5 eV, which is among the largest SOC strengths ever observed in a bulk material, and this represents the origin of many exotic physical phenomena emerging from the unusually intricate interplay between the spin, charge and orbital degrees of freedom, explicated by the formation of a multipolar magnetic state associated with tilted orbital ordering in the f-orbital manifold. Finally, we have uncovered the role of dipole-dipole and quadrupole-quadrupole spin interactions in the formation of the non-collinear 3**k** state and

ruled out Jahn-Teller distortions as a factor in stabilizing the 3**k** magnetic ordering. The most relevant energy scales defining the properties of UO_2 are summarized in Table VII.

Besides elucidating the complexity of exotic physical scenarios, these results provide a solid reference for future studies of relativistic non-collinear materials (in particular 5d transition metal oxides), and open the way to a quantitatively reliable exploration of technologically relevant aspects of UO_2 such as spin and orbital magnetic dynamics, formation and evolution of structural defects and their diffusion, which is a topic of significant importance to applications. From this perspective, the study represents an example on how an accurate account of fundamental microscopic interactions derived from a direct application of laws of quantum mechanics can provide an accurate quantitative account of a number of physical processes and extract values of critical parameters that can then be used as input for phenomenological schemes describing macroscopic phenomena such as transport and dissipation.

[1] J. Kubler, K. H. Hock, J. Sticht, and A. R. Williams, Journal of Physics F: Metal Physics **18**, 469 (1988).

[2] L. M. Sandratskii, Advances in Physics **47**, 91 (1998).

[3] T. Yamada, N. Kunitomi, Y. Nakai, D. E. Cox, and G. Shirane, Journal of the Physical Society of Japan **28**, 615 (1970), https://doi.org/10.1143/JPSJ.28.615.

[4] S. Heinze, M. Bode, A. Kubetzka, O. Pietzsch, X. Nie, S. Blügel, and R. Wiesendanger, Science **288**, 1805 (2000), http://science.sciencemag.org/content/288/5472/1805.full.pdf.

[5] H. Ohldag, A. Scholl, F. Nolting, S. Anders, F. U. Hillebrecht, and J. Stöhr, Phys. Rev. Lett. **86**, 2878 (2001).

[6] N. Hauptmann, J. W. Gerritsen, D. Wegner, and A. A. Khajetoorians, Nano Letters **17**, 5660 (2017).

[7] J. Faber and G. H. Lander, Phys. Rev. B **14**, 1151 (1976).

[8] P. Burlet, J. Rossat-Mignod, S. Quezel, O. Vogt, J. C. Spirlet, and J. Rebizant, Journal of the Less Common Metals **121**, 121 (1986), proceedings of Actinides 85, Aix en Provence, September 2-6, 1985.

[9] P. Giannozzi and P. Erd??s, Journal of Magnetism and Magnetic Materials **67**, 75 (1987).

[10] G. Jackeli and G. Khaliullin, Phys. Rev. Lett. **102**, 017205 (2009).

[11] P. Liu, S. Khmelevskyi, B. Kim, M. Marsman, D. Li, X.-Q. Chen, D. D. Sarma, G. Kresse, and C. Franchini, Phys. Rev. B **92**, 054428 (2015).

[12] A. A. Starikov, Y. Liu, Z. Yuan, and P. J. Kelly, Phys. Rev. B **97**, 214415 (2018).

[13] B. Kim, P. Liu, Z. Ergönenc, A. Toschi, S. Khmelevskyi, and C. Franchini, Phys. Rev. B **94**, 241113 (2016).

[14] B. Kim, S. Khmelevskyi, I. I. Mazin, D. F. Agterberg, and C. Franchini, npj Quantum Materials **2**, 37 (2017).

[15] K. Gofryk, S. Du, C. R. Stanek, J. C. Lashley, X. Y. Liu, R. K. Schulze, J. L. Smith, D. J. Safarik, D. D. Byler, K. J. McClellan, B. P. Uberuaga, B. L. Scott, and D. A. Andersson, Nat Commun **5**, 4551 (2014).

[16] M. Jaime, A. Saul, M. Salamon, V. S. Zapf, N. Harrison, T. Durakiewicz, J. C. Lashley, D. A. Andersson, C. R. Stanek, J. L. Smith, and K. Gofryk, Nature Communications **8**, 99 (2017).

[17] P.-W. Ma, S. L. Dudarev, and C. H. Woo, Computer Physics Communications **207**, 350 (2016).

[18] P. W. Anderson, Phys. Rev. **79**, 350 (1950).

[19] P. W. Anderson, Phys. Rev. **115**, 2 (1959).

[20] A. Kotani and T. Yamazaki, Progress of Theoretical Physics Supplement **108**, 117 (1992).

[21] V. Mironov, L. Chibotaru, and A. Ceulemans, in *Advances in Quantum Chemistry*, Advances in Quantum Chemistry, Vol. 44 (Academic Press, 2003) pp. 599 – 616.

[22] S.-T. Pi, R. Nanguneri, and S. Y. Savrasov, Phys. Rev. Lett. **112**, 077203 (2014).

[23] S.-T. Pi, R. Nanguneri, and S. Savrasov, Phys. Rev. B **90**, 045148 (2014).

[24] S. L. Dudarev, G. A. Botton, S. Y. Savrasov, C. J. Humphreys, and A. P. Sutton, Phys. Rev. B **57**, 1505 (1998).

[25] V. I. Anisimov, J. Zaanen, and O. K. Andersen, Phys. Rev. B **44**, 943 (1991).

[26] D. Nguyen-Manh and S. L. Dudarev, Phys. Rev. B **80**, 104440 (2009).

[27] A. I. Liechtenstein, V. I. Anisimov, and J. Zaanen, Phys. Rev. B **52**, R5467 (1995).

[28] V. I. Anisimov, F. Aryasetiawan, and A. I. Lichtenstein, Journal of Physics: Condensed Matter **9**, 767 (1997).

[29] M. Cococcioni, *The LDA+U Approach: A Simple Hubbard Correction for Correlated Ground States* (in: E. Pavarini, E. Koch, F. Anders, and M. Jarrell (Eds.), Correlated Electrons: From Models to Materials Modeling and Simulation, Vol. 2 Forschungszentrum Julich, 2012).

[30] V. V. Mazurenko, S. L. Skornyakov, A. V. Kozhevnikov, F. Mila, and V. I. Anisimov, Phys. Rev. B **75**, 224408 (2007).

[31] E. R. Ylvisaker, W. E. Pickett, and K. Koepernik, Phys. Rev. B **79**, 035103 (2009).

[32] E. Bousquet and N. Spaldin, Phys. Rev. B **82**, 220402 (2010).

[33] T. A. Mellan, F. Corà, R. Grau-Crespo, and S. Ismail-Beigi, Phys. Rev. B **92**, 085151 (2015).

[34] M. E. A. Coury, S. L. Dudarev, W. M. C. Foulkes, A. P. Horsfield, P.-W. Ma, and J. S. Spencer, Phys. Rev. B **93**, 075101 (2016).

[35] S. J. Allen, Phys. Rev. **166**, 530 (1968).

[36] S. J. Allen, Phys. Rev. **167**, 492 (1968).

[37] C. R., A. G., S. P., L. G. H., K. J., and de V. Du Plessis P., Phys. Rev. B **59**, 13892 (1999).

[38] R. Laskowski, G. K. H. Madsen, P. Blaha, and K. Schwarz, Phys. Rev. B **69**, 140408 (2004).

[39] F. Zhou and V. Ozoliņš, Phys. Rev. B **83**, 085106 (2011).

[40] M. A. Korotin, Z. V. Pchelkina, N. A. Skorikov, A. V. Efremov, and V. I. Anisimov, Theory of Metals **117**, 655 (2016).

[41] J. T. Pegg, X. Aparicio-Angles, M. Storr, and N. H. de Leeuw, Journal of Nuclear Materials **492**, 269 (2017).

[42] F. Bruneval, M. Freyss, and J.-P. Crocombette, Phys. Rev. Materials **2**, 023801 (2018).

[43] J. P. Crocombette, F. Jollet, L. T. Nga, and T. Petit, Phys. Rev. B **64**, 104107 (2001).

[44] B. Dorado, D. A. Andersson, C. R. Stanek, M. Bertolus, B. P. Uberuaga, G. Martin, M. Freyss, and P. Garcia, Phys. Rev. B **86**, 035110 (2012).

[45] E. Vathonne, D. A. Andersson, M. Freyss, R. Perriott, M. W. D. Cooper, C. R. Stanek, and M. Bertolus, Inorganic Chemistry **56**, 125 (2017).

[46] X.-Y. Liu and D. A. Andersson, Journal of Nuclear Materials **498**, 373 (2018).

[47] D. Nguyen-Manh, A. P. Horsfield, and S. L. Dudarev, Phys. Rev. B **73**, 020101 (2006).

[48] H. Wen, P.-W. Ma, and C. Woo, Journal of Nuclear Materials **440**, 428 (2013).

[49] R. Caciuffo, P. Santini, S. Carretta, G. Amoretti, A. Hiess, N. Magnani, L.-P. Regnault, and G. H. Lander, Phys. Rev. B **84**, 104409 (2011).

[50] P.-W. Ma, C. H. Woo, and S. L. Dudarev, Physical Review B **78**, 024434 (2008).

[51] J. Tranchida, S. J. Plimpton, P. Thibaudeau, and A. P. Thompson, Journal of Computational Physics **372**, 406 (2018).

[52] B. Dorado, M. Freyss, B. Amadon, M. Bertolus, G. Jomard, and P. Garcia, J. Phys.:Condens. Matter **25**, 333201 (2013).

[53] S. L. Dudarev, M. R. Castell, G. A. Botton, S. Y. Savrasov, C. Muggelberg, G. A. D. Briggs, A. P. Sutton, and D. T. Goddard, Micron **31**, 363 (2000).

[54] K. Sasaki and Y. Obata, Journal of the Physical Society of Japan **28**, 1157 (1970).

[55] C. Franchini, R. Podloucky, J. Paier, M. Marsman, and G. Kresse, Phys. Rev. B **75**, 195128 (2007).

[56] F. Aryasetiawan, K. Karlsson, O. Jepsen, and U. Schönberger, Phys. Rev. B **74**, 125106 (2006).

[57] M. Cococcioni and S. de Gironcoli, Phys. Rev. B **71**, 035105 (2005).

[58] I. V. Solovyev, Phys. Rev. B **73**, 155117 (2006).

[59] V. I. Anisimov and O. Gunnarsson, Phys. Rev. B **43**, 7570 (1991).

[60] L. Vaugier, H. Jiang, and S. Biermann, Phys. Rev. B **86**, 165105 (2012).

[61] B. Kim, P. Liu, and C. Franchini, Phys. Rev. B **95**, 115111 (2017).

[62] B. Kim, P. Liu, J. M. Tomczak, and C. Franchini, Phys. Rev. B **98**, 075130 (2018).

[63] P. Liu, B. Kim, X.-Q. Chen, D. D. Sarma, G. Kresse, and C. Franchini, Phys. Rev. Materials **2**, 075003 (2018).

[64] S. L. Dudarev and P. M. Derlet, Journal of Computer-Aided Materials Design **14**, 129 (2007).

[65] B. Caroli, C. Caroli, and D. R. Fredkin, Phys. Rev. **178**, 599 (1969).

[66] A. M. Kosevich, The Crystal Lattice: Phonons, Solitons, Dislocations (Wiley-VCH Weinheim, Berlin, 1999).

[67] J. Hubbard, Proceedings of the Royal Society of London A: Mathematical, Physical and Engineering Sciences **276**, 238 (1963).

[68] G. Kresse and J. Hafner, Phys. Rev. B **47**, 558 (1993).

[69] G. Kresse and J. Furthmüller, Phys. Rev. B **54**, 11169 (1996).

[70] O. Bengone, M. Alouani, P. Blöchl, and J. Hugel, Phys. Rev. B **62**, 16392 (2000).

[71] D. Hobbs, G. Kresse, and J. Hafner, Phys. Rev. B **62**, 11556 (2000).

[72] A. Momin, E. Mirza, and M. Mathews, Journal of Nuclear Materials **185**, 308 (1991).

[73] S. L. Dudarev, D. Nguyen-Manh, and A. P. Sutton, Philosophical Magazine B **75**, 613 (1997).

[74] P.-W. Ma and S. L. Dudarev, Phys. Rev. B **91**, 054420 (2015).

[75] B. Dorado, B. Amadon, M. Freyss, and M. Bertolus, Phys. Rev. B **79**, 235125 (2009).

[76] B. Meredig, A. Thompson, H. A. Hansen, C. Wolverton, and A. van de Walle, Phys. Rev. B **82**, 195128 (2010).

[77] J. P. Allen and G. W. Watson, Phys. Chem. Chem. Phys. **16**, 21016 (2014).

[78] A. Arima, M. Harvey, and K. Shimizu, Physics Letters B **30**, 517 (1969).

[79] M. Pryce, Proc. Phys. Soc. (London) **25** (1950).

[80] M. A. Abragam, A.Pryce, Proc. Phys. Soc. (London) **135** (1951).

[81] L. F. Chibotaru, "Ab initio methodology for pseudospin hamiltonians of anisotropic magnetic complexes," in Advances in Chemical Physics (Wiley-Blackwell, 2013) pp. 397–519.

[82] J. Sakurai, Modern Quantum Mechanics (Addison-Wesley, Reading, MA, 1993).

[83] P. Santini, S. Carretta, G. Amoretti, R. Caciuffo, N. Magnani, and G. H. Lander, Rev. Mod. Phys. **81**, 807 (2009).

[84] S. Carretta, P. Santini, R. Caciuffo, and G. Amoretti, Phys. Rev. Lett. **105**, 167201 (2010).

[85] In this supplementary material, we provide the coordinates of S_A and S_B spins that define the six inequivalent AB pairs within the local quantization axis x, y, and z as defined in Fig. 3.

[86] M. D. Jones and R. C. Albers, Phys. Rev. B **79**, 045107 (2009).

[87] B. Andlauer, J. Schneider, and W. Tolksdorf, physica status solidi (b) **73**, 533 (1976).

[88] G. Amoretti, A. Blaise, R. Caciuffo, J. M. Fournier, M. T. Hutchings, R. Osborn, and A. D. Taylor, Phys. Rev. B **40**, 1856 (1989).

[89] J. Schoenes, Physics Reports **63**, 301 (1980).

[90] B. C. Frazer, G. Shirane, D. E. Cox, and C. E. Olsen, Phys. Rev. **140**, A1448 (1965).

[91] J. B. M. Goodenough, Magnetism And The Chemical Bond (John Wiley And Sons, 1963).

[92] L. V. Pourovskii and S. Khmelevskyi, arXiv:1810.05484 (2018).

[93] J. von Neumann, With four parameters I can fit an elephant, and with five I can make him wiggle his trunk.